Malaysian Journal of Chemistry, 2024, Vol. 26(5), 185-193
(Special Issue: *3rd Virtual International Symposium on Sciences 2023*)

The Morphological and Structural Properties of Chromium (Cr)-doped Titanium Dioxide (TiO_2) Nanoparticles prepared via Sol–gel Method at Various Concentrations

Nurul Huda Mohd Noor[1,2], Nur Syaza Sahira M. N. Jaya Saputra[2], Suraya Ahmad Kamil[2,3], Mohamad Rusop Mahmood[3,4], Aida Fazliza Mat Fadzil[1,2,3] and Siti Nurbaya Supardan[2,3]*

[1]Centre of Foundation Studies, Universiti Teknologi MARA, Cawangan Selangor, Kampus Dengkil, 43800 Dengkil, Selangor, Malaysia
[2]Faculty of Applied Sciences, Universiti Teknologi MARA, 40450 Shah Alam, Selangor, Malaysia
[3]Centre for Functional Materials and Nanotechnology, Institute of Science (IoS), Universiti Teknologi MARA, 40450 Shah Alam, Selangor, Malaysia
[4]NANO-Electronic Centre, College of Engineering, Universiti Teknologi MARA, 40450 Shah Alam, Selangor, Malaysia
*Corresponding author (e-mail: sitinurbaya86@uitm.edu.my)

Titanium dioxide (TiO_2) is a widely studied material and is commonly used as a photocatalyst due to its strong oxidation capability and resistance to chemical corrosion and photocorrosion. However, its large band gap and quick recombination of photo-generated electron–hole pairs lead to numerous disadvantages that reduce photocatalytic performance. One of the promising strategies to overcome these issues is by doping TiO_2 with metal ions. In this study, pure TiO_2 and chromium (Cr)-doped TiO_2 nanoparticles with various doping concentrations (1, 3, and 5 wt%) were successfully prepared by a sol–gel method. All samples were characterized using field emission scanning electron spectroscopy (FESEM), X-ray diffraction (XRD), and Fourier transform infrared (FTIR) spectroscopy. The surface morphology of pure and Cr-doped TiO_2 nanoparticles shows an agglomeration of spherical shape. The XRD analysis showed that a mixed phase of anatase and rutile started to appear at 1 wt% Cr and the phases remained unchanged until 5 wt% compared to pure TiO_2 sample, which showed anatase phase only. The crystallite size of anatase TiO_2 decreased from 69.55 to 17.38 nm with 1 wt% Cr doping, whereas the crystallite size of rutile in Cr-doped TiO_2 increased slightly from 22.22 nm for 1 wt% to 38.08 nm for 3 wt%. The specific surface area (SSA) for the anatase TiO_2 sample was 22.01 m^2/g and increased to the highest value of 88.05 m^2/g with 1 wt% Cr doping, whereas the highest SSA for rutile was 64.44 m^2/g in 1 wt% Cr-doped TiO_2. The results indicate that Cr plays an important role in the modification of the structural characteristics of TiO_2 nanoparticles.

Keywords: Titanium dioxide (TiO_2); Chromium; Cr-doped TiO_2; sol–gel; structural property

Received: November 2023; Accepted: February 2024

Titanium dioxide (TiO_2) is a widely studied material with various applications in different fields. It is commonly used as a photocatalyst due to its strong oxidation capability and resistance to chemical corrosion and photocorrosion [1]. Nanostructured semiconductors show great potential for environmental remediation because of photocatalytic oxidation, which is activated under solar light or ultraviolet (UV) light [2]. The most crystalline forms of TiO_2 are anatase and rutile; anatase is commonly used in air and water cleaning systems because of its excellent photocatalytic properties [3]. Photocatalysis for water and air purification has received substantial focus in research, and its applications have recently expanded to surfaces with self-cleaning, self-sterilizing, and bactericidal anti-fog properties [4]. The different crystalline forms exhibit varying levels of reactivity and efficiency in different applications. For example, mixed polymorphs of TiO_2 have been shown to be more efficient for biomedical applications than single crystals [5]. Other studies reported that among the TiO_2 structures, anatase is commonly preferred since it is more efficient for light-harvesting processes, photocatalytic applications, and more recently, in dye-sensitized and perovskite solar cells [6]. Anatase TiO_2 has a large band gap energy of 3.2 eV which corresponds to a wavelength of 385 nm; electron hole–pairs are generated when TiO_2 is exposed to this wavelength of light. However, TiO_2 is not an efficient photocatalyst because of its large bandgap energy that only allows operation within the UV range and high electron–hole recombination rate, which retains a limited amount of hydroxyl species on its surface [7].

Many efforts have been made to improve the photocatalytic efficiency of TiO_2 under both UV and visible light irradiation. Surface changes and dopant introduction into the TiO_2 lattice are simple yet

†Paper presented at the 3rd Virtual International Symposium on Sciences (3rd VISoS 2023)

effective methods. Doping is an effective approach to modify and enhance the electronic and optical properties of TiO_2 and reduce the recombination of the electron–hole pairs. A wide range of metal ions, particularly transition metal ions such as iron (Fe), nickel (Ni), copper (Cu), manganese (Mn), cobalt (Co), and chromium (Cr), have been used as dopants for TiO_2 [8]. Cr has been widely used as dopant since Cr doping can narrow the band gap and extend the photoresponse to the visible light range [9]. A previous study showed that doping with Cr^{3+} ions decreased the crystal size of TiO_2 and shifted the valence band maximum upward, leading to strong visible-light absorption [7]. Cr-doped TiO_2 exhibits unique optical properties that make it suitable for various applications, particularly in photocatalysis. Moreover, Cr not only modifies the optical properties of TiO_2 by extending the absorption edge to the visible region, it also improves the photocurrent density that makes TiO_2 nanoparticles (NPs) suitable for photocatalytic activity, air and water purification, and solar cell applications.

A previous study by Choudhury and Choudhury [10] concluded that the interaction of Cr^{3+} with lattice Ti^{4+} changes with different Cr^{3+} concentrations. The anomalous changes in lattice parameters with Cr^{3+} content clearly indicate that the structural distortion is affected not only by substitutional doping but also by interstitial Cr^{3+} and oxygen vacancies, which has been confirmed by Raman spectroscopy. Furthermore, the alteration of octahedral symmetry on Cr^{3+} incorporation into the lattice site of TiO_2 is the cause of the absence of a strong emission line of Cr^{3+} at 688 nm [10]. Researchers have used several techniques to prepare TiO_2 powder such as chemical bath deposition, ultrasonic spray pyrolysis, liquid phase deposition, and sol–gel method [11]. The sol–gel method is a promising technique for the most efficient production of powder. At low reaction temperatures, sol–gel has the capability to derive metastable structure and excellent chemical homogeneity. The sol–gel process typically consists of catalyzed hydrolysis and condensation processes with small molecules, leading to the transformation of an intricate network.

EXPERIMENTAL

Chemicals and Materials

The following reagents were used as received without additional purification: titanium(IV) butoxide (TTIB) (Aldrich, 97%), ethanol (C_2H_5OH), chromium(III) nitrate nonahydrate ($Cr(NO_3)_3{\cdot}9H_2O$) (Aldrich, 99%), 1 M nitric acid (HNO_3), and deionized water.

Preparation Method

TiO_2 NPs were synthesized via sol–gel technique at room temperature (25 °C) following Mathews et al. [12] with some modifications. A mixture of 5 mL deionized water and 55 mL ethanol was added dropwise into a solution containing 26 mL titanium (IV) butoxide and 55 mL ethanol and stirred for 1 h. The solution was continuously stirred for another 4 h at room temperature (25 °C) at 200–400 rpm. The acidity of the solution was controlled by adding HNO_3 dropwise to attain pH of 2.0. Then, the solution was stirred for another 1 h. For the solution with Cr doping, the amount of $Cr(NO_3)_3$ with 1, 3, and 5 wt% was added into the precursor of Cr-doped TiO_2, and it was peptized overnight to get 2 layers of the solution. The solution was filtered to obtain the titanic gel, which was dried on a hot plate at 120 °C for 1.5 h until it formed a powder. The powder was pulverized using ball milling at 900 rpm for 3 h to obtain TiO_2 NPs. The powder samples were calcined at 500 °C for 3 h at a heating rate of 5 °C/min.

Characterization Methods

The morphology and composition of the prepared samples were assessed by field emission scanning electron microscopy (FESEM) using SUPRA 40VP by ZEISS.XRD technique (PANalytical X'Pert Pro). Cu Kα radiation was employed to determine the phase and crystal structure of TiO_2 NPs. The diffractometer data were recorded by scanning the sample through a range of 2θ angles. The average crystallite size (D) for TiO_2 NPs was calculated by using the Debye–Scherrer equation from the XRD analysis [13][14] using Equation (1). This equation is a well-known method for calculating the crystallite size based on the line broadening for the XRD peaks at their full width at half maximum (FWHM).

$$D = \frac{0.9\lambda}{\beta \cos\theta} D = \frac{0.9\lambda}{\beta \cos\theta} \quad (1)$$

where λ is the X-ray wavelength, 0.9 is the Scherrer constant, β is FWHM, and θ is the corresponding diffraction angle.

FTIR was used to determine the molecular structure and chemical bonding in the prepared samples [15]. FTIR spectrum can be divided into two regions: functional group region and fingerprint region. The specific functional groups in a sample can be determined in the wavenumber range of 4000 to 1500 cm^{-1}, while the fingerprint region can be examined from 1500 to 500 cm^{-1}. The sample transmission represents the light absorbed by the molecule. The energy from the light causes the bond to vibrate, and the bond vibration can be divided into several types such as bond stretching, bending, rocking, and twisting. The functional groups have their respective wavenumber [11]. Therefore, the peak present at the wavenumber in the functional group region can be characterized by comparing it with the standard wavenumber of the functional group. FTIR spectrometer (Perkin Elmer Spectrum 400 FTIR/FT-NIR) was used to measure the transmission of the sample with a scan range of 4000–450 cm^{-1}.

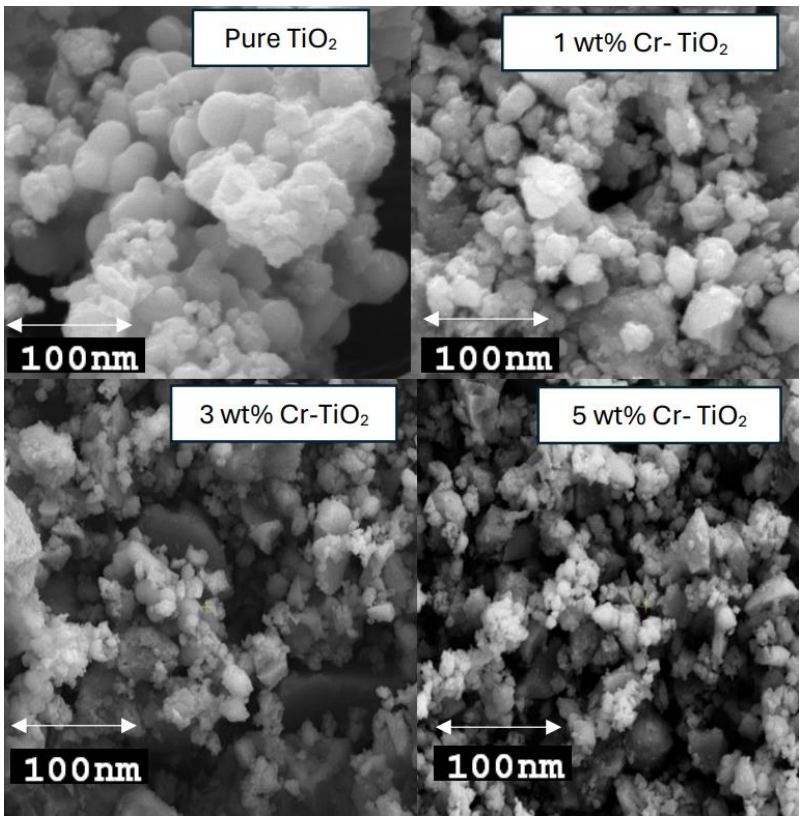

Figure 1. FESEM images of pure TiO_2, 1 wt% Cr–TiO_2, 3 wt% Cr–TiO_2, and 5 wt% Cr–TiO_2 NPs.

RESULTS AND DISCUSSION

Field Emission Scanning Electron Microscopy (FESEM)

FESEM is an effective method for examining nanoparticle surface morphology. The synthesis method and surface chemistry affect sample stability. All synthesized particles have spherical shapes, non-uniform sizes, and a high degree of agglomeration, which could be due to the presence of both water molecules and hydroxyl group [16]. The pure and Cr-doped TiO_2 NPs are spherical and highly agglomerated (Figure 1). Cr-doped TiO_2 have smaller sizes compared to pure TiO_2, where they ranged from 88.5 to 22.5 nm. Moreover, the degree of agglomeration decreased as Cr concentration increased.

X-Ray Diffraction (XRD)

The crystal phase and crystallite size of pure and Cr-doped TiO_2 NPs were investigated, and their XRD diffraction patterns are shown in Figure 2. The diffraction patterns were compared to the ICSD using POWD-12++ (1997). The anatase phase peaks were observed at 2θ values of 25.37°, 38.67°, 48.16°, 54.05°, 55.20°, 62.87°, 68.98°, 70.48°, 75.28°, and 83.40° that correspond to the crystal planes of (101), (112), (200), (105), (211), (204), (116), (220), (215), and (312) respectively. Meanwhile, the rutile phase peaks were observed at 2θ values of 27.43°, 54.32°, and 69.00° corresponding to the crystal planes of (210), (211), and (301) respectively. The peaks fluctuated with different concentrations of Cr, as the doping affected the phase composition of anatase and rutile. Cr doping is needed to induce crystal growth, thus different concentrations were tested to achieve complete crystallization. Pure TiO_2 NPs have the structural phase of anatase (Figure 2). Cr doping resulted in a mixture of anatase and rutile phases, in which anatase dominated as the Cr concentration increased from 1 to 5 wt%. The rutile phase appeared at peaks (210), (211), and (301). This is because the oxygen defect levels significantly impact the kinetics of anatase-to-rutile conversion, and changes in oxygen vacancy promote the transformation [17]. Next, as the concentration increased from 1 to 3 wt%, the peak of rutile at (210) disappeared because sometimes the grains are not oriented in the correct way to allow diffraction from the planes, while other rutile peaks remained unchanged. Therefore, it can be suggested that the presence of Cr in the anatase crystal lattice in place of 4 valent Ti makes the combination of anatase and rutile phase achievable because it creates more oxygen vacancies that will assist the mass transport required for a complete transformation into rutile [17].

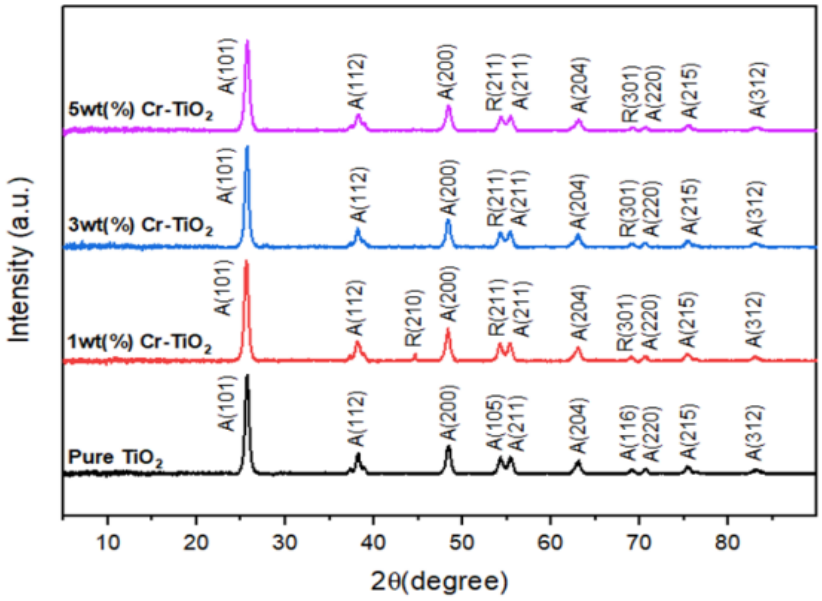

Figure 2. XRD diffraction patterns of pure and Cr-doped TiO_2 NPs with different concentrations with anatase (A) and rutile (R) phases.

$$W_R = \frac{1}{1+0.8\left(\frac{I_A}{I_R}\right)} \quad W_R = \frac{1}{1+0.8\left(\frac{I_A}{I_R}\right)} \tag{2}$$

$$W_A\, W_A = 1 - W_R = 1 - W_R \tag{3}$$

$$Anatase\ \% = \frac{100 \times I_A}{I_A + 1.265 \times I_R} Anatase\ \% = \frac{100 \times I_A}{I_A + 1.265 \times I_R} \tag{4}$$

$$100 - A\% = Rutile\ \% 100 - A\% = Rutile\ \% \tag{5}$$

$$SSA = \frac{6\times10^3}{\rho D_p} SSA = \frac{6\times10^3}{\rho D_p} \tag{6}$$

$$\rho = \frac{1}{{D_p}^2} \rho = \frac{1}{{D_p}^2} \tag{7}$$

The mole ratios of the anatase and rutile phases were calculated based on the equations by Spurr and Myers as represented in Equations (2) and (3) [14] using the most intense peak of each phase. Next, the specific surface area (SSA) was calculated as the total area covered by the crystals in unit mass as shown in Equation (6). The density is denoted by ρ, while D_p denotes the size of the crystals obtained from the Debye–Scherrer equation.

W_R and I_R represent the mole fraction and intensity of the rutile phase, respectively, while W_A and I_A are the mole fraction and intensity of the anatase phase, respectively. The phase contents of anatase (101) and rutile (110) were obtained using Equations (4) and (5). I_A and I_R represent the intensity of the anatase (101) and rutile (211) phases, respectively. Table 1 shows the quantitative results of the XRD analysis.

The XRD patterns were utilized to determine the weight fraction of anatase and rutile. The ratio of anatase to rutile was calculated by inserting the values I_A and I_R in Spurr and Myers's equation, and the ratio is shown in Figure 3. The ratios of anatase to rutile for pure and Cr-doped TiO_2 at 1, 3, and 5 wt% were 100:0, 82.32:17.68, 84.49:15.51, and 84.44:15.56, respectively, proving the anatase-to-rutile phase transformation occurred due to the increase in Cr concentration.

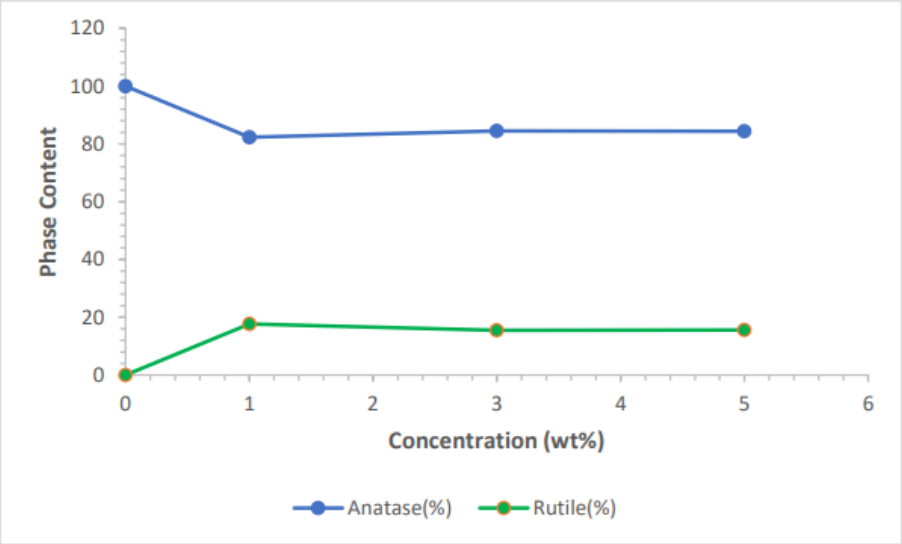

Figure 3. Phase content of pure and Cr-doped TiO_2 NPs with different concentrations.

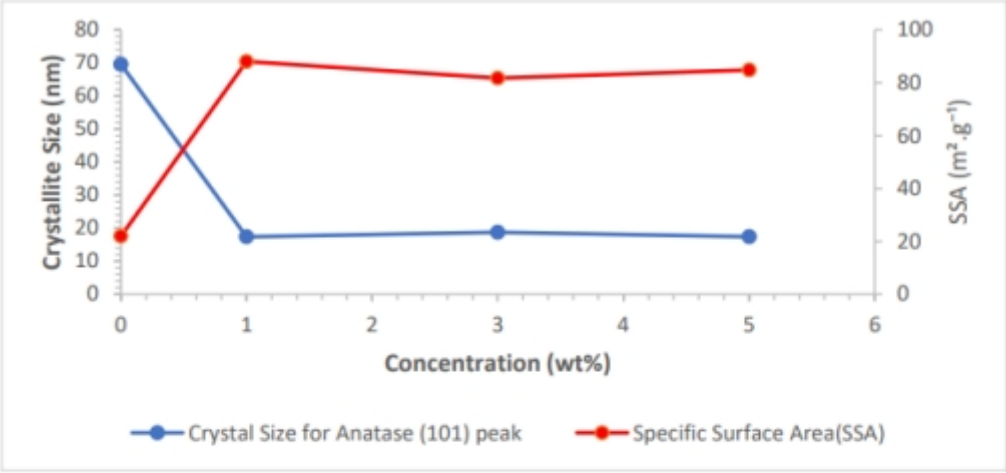

(a)

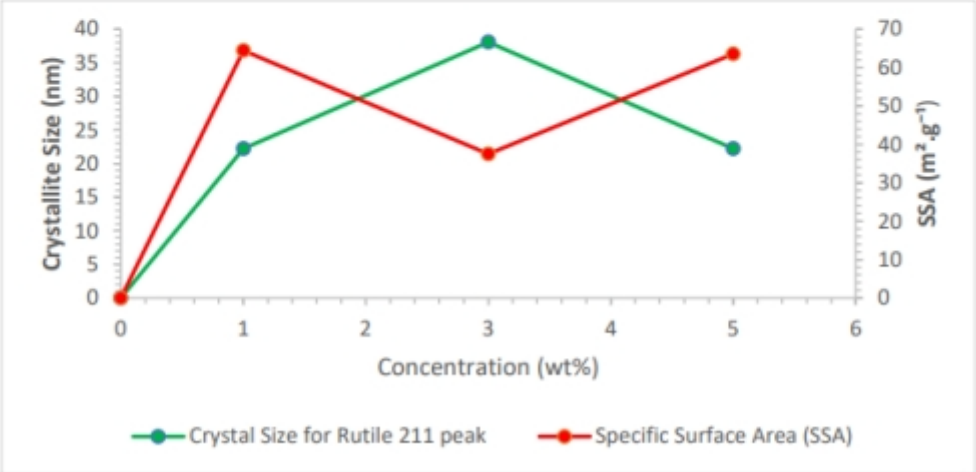

(b)

Figure 4. Specific surface area of (a) anatase (b) rutile for pure and Cr-doped TiO_2 NPs.

Figure 4 shows the SSA of anatase and rutile for pure and Cr-doped TiO_2. The densities (ρ) for anatase are 3.92, 3.92, 3.92, and 4.07 g/m^3 while for rutile are 4.23, 4.19, 4.20, and 4.25 g/m^3 in TiO_2 for pure and Cr-doped at 1, 3, and 5 wt%, respectively. The SSA value increased from 22.01 to 88.05 m^2/g for anatase and from 0 to 64.44 m^2/g for rutile with the addition of 1 wt% Cr to 63.52 m^2/g (Table 1). The addition of 3 wt% Cr increased the crystallite size for rutile from 22.2 to 38.08 nm and reduced the SSA from 64.44 to 37.52 m^2/g; this might lower the photocatalytic efficiency. Conversely, an increase in SSA along with decreased crystallite size would increase the reactant's adsorption on the photocatalyst and light absorption. Hence, the higher surface area can help to improve the photocatalysis process due to the crystallite size [13].

Table 1. Quantitative results of XRD diffraction pattern analysis of Cr-doped TiO_2 NPs.

Cr (wt%)	FWHM (β)		Crystallite size		Phase content (%)		Specific surface area, SSA (m²/g)	
	Anatase (101)	Rutile (211)	Anatase (101)	Rutile (211)	Anatase (101)	Rutile (211)	Anatase (101)	Rutile (211)
0	0.1171	0	69.55	0	100	0	22.01	0
1	0.4684	0.4015	17.38	22.22	82.32	17.68	88.05	64.44
3	0.4349	0.2342	18.73	38.08	84.49	15.51	81.73	37.52
5	0.4684	0.4015	17.39	22.23	84.44	15.56	84.77	63.52

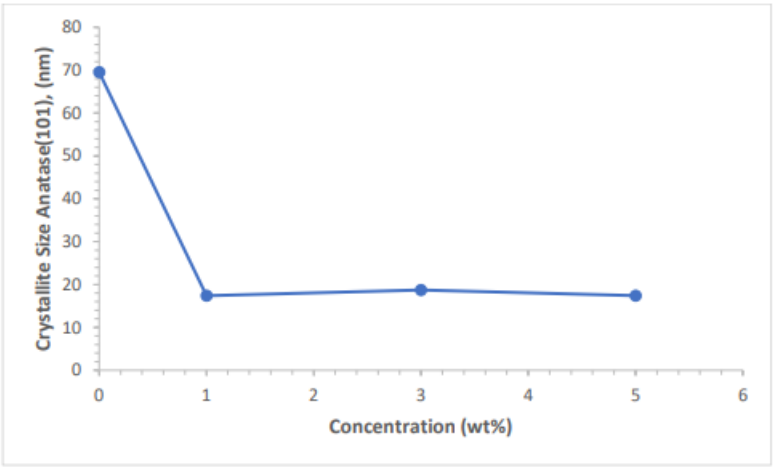

(a)

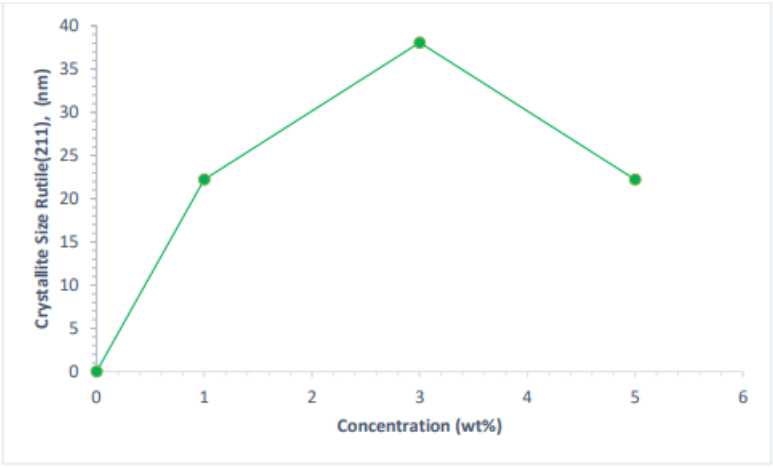

(b)

Figure 5. Crystallite size of (a) anatase and (b) rutile in pure and Cr-doped TiO_2 NPs calculated using Debye–Scherrer equation.

The crystallite sizes of pure and Cr-doped TiO_2 NPs were determined based on the full width at half maximum (FWHM) values calculated using Debye–Scherrer equation. Compared with pure TiO_2, the FWHM of the XRD peaks were higher for the Cr-doped samples. The anatase in Cr-doped TiO_2 samples decreased in intensity with increasing FWHM of the Bragg peak. The crystallite size of anatase decreased from 69.55 nm for pure TiO_2 to 17.38, 18.73, and 17.39 nm for 1, 3, and 5 wt% Cr-doped TiO_2, respectively. Meanwhile, the crystallite size of rutile increased from 22.22 to 38.08 nm from 1 to 3 wt% and then decreased to 22.23 nm with the addition of 5 wt% Cr as shown in Figure 5. Some dopants may have been prevented from entering the octahedral position of the lattice and remained on the grain boundaries or surface. As a result, the lattice's periodicity was interrupted, which affected crystal development and reduced crystallite size [18]. The rutile phase started appearing when the anatase phase decreased; this resulted in a mixed phase state that can improve the photocatalysis process.

The FWHM of the XRD peaks of doped samples increased in comparison with that of the pure TiO_2 sample, indicating that crystallite size decrease due to Cr doping is proportional to the FWHM. Figure 6 shows the relationship of FWHM with crystallite size. As Cr concentration increased, there may be an increase in structural flaws that inhibited the grain from growing. This may result in a small number of oxygen vacancies moving to the surface or grain boundary that restrict crystallite growth and limit crystallite size. These structural flaws may influence the material's crystallites size while lowering the peak intensity [10].

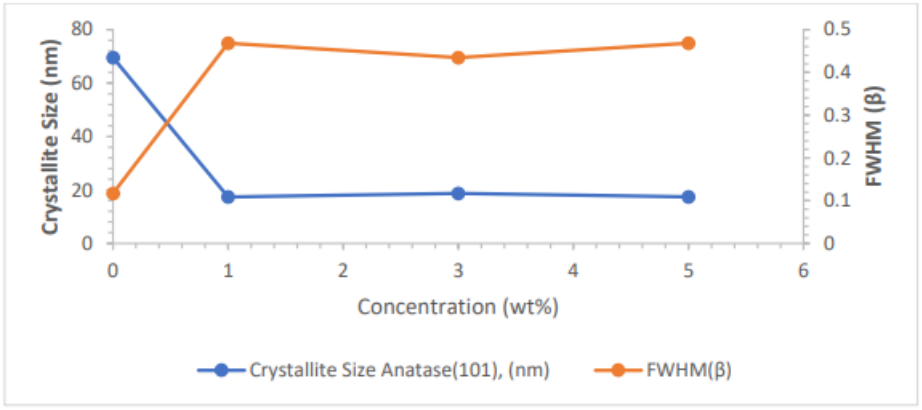

(a)

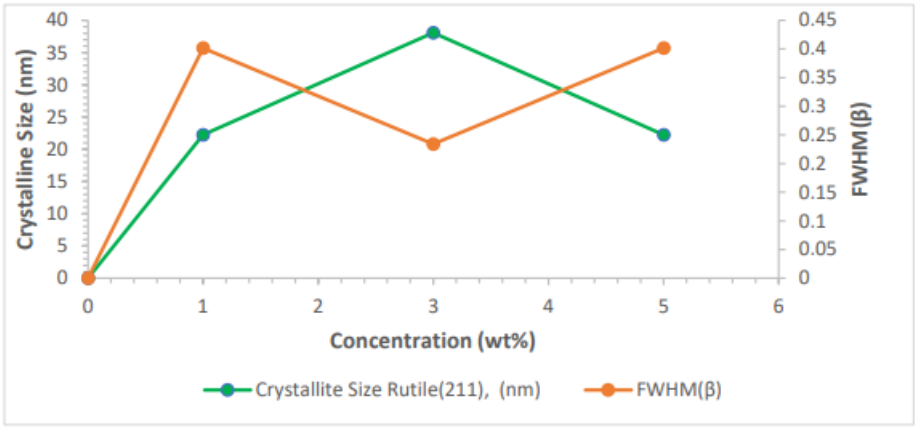

(b)

Figure 6. FWHM vs crystallite size of (a) anatase (b) rutile

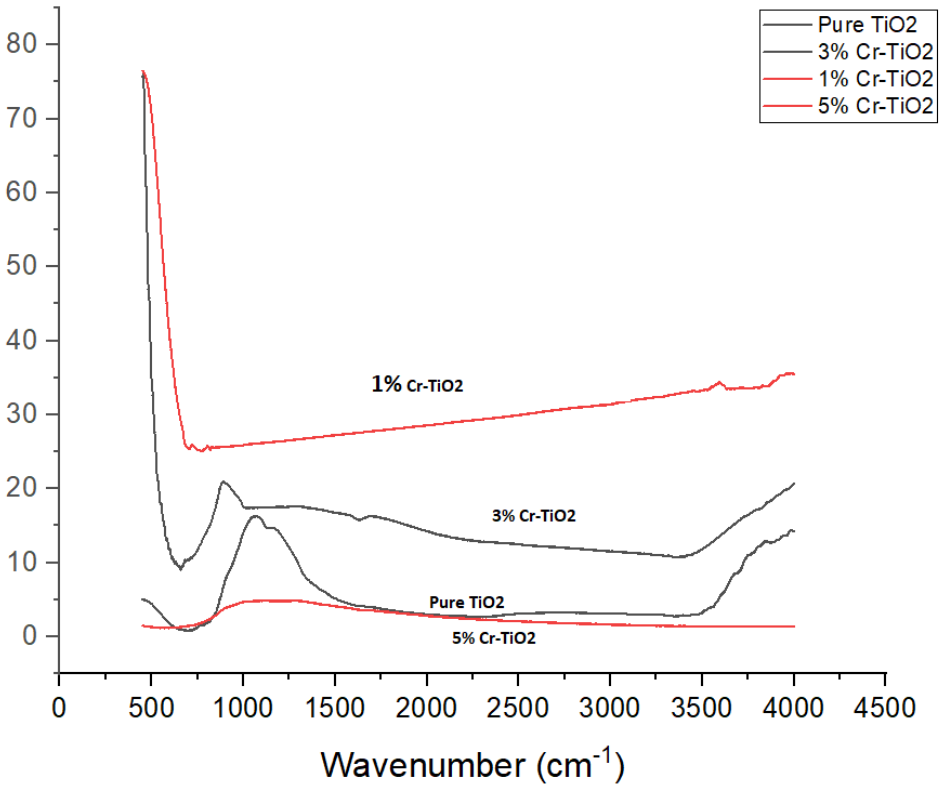

Figure 7. FTIR spectra of pure and Cr-doped TiO_2 NPs.

Fourier Transform Infrared (FTIR)

Figure 7 shows the absorption spectra of pure and Cr-doped TiO_2 NPs calcined at different concentrations in the region of 4000–500 cm^{-1}. The peaks in this region are characteristic of infrared (IR)-active fundamental and combination lattice modes of crystalline Cr and Ti oxides [11]. The peak intensity and band position depend on the crystal structure, chemical composition, and sample morphology [19]. The peak positions in an IR spectrum are used to distinguish different functional groups from each other. Different functional groups can have peaks at about the same position. Generally, metal oxides show peaks in the fingerprint region, which in the range of 1500 to 500 cm^{-1} [20]. The peak in the range 3352–3820 cm^{-1} [15][21] corresponds to the bending and stretching modes of the –OH groups of absorbed molecular water, indicating that the sample is hydrolyzed [22]. The wide band in the range of 450–700 cm^{-1} combines stretching modes of Ti–O–Ti bonds which are typical for titanium oxides [15]. The band around 548–698 cm^{-1} is attributed to Ti–O stretching vibration. The 698.0 cm^{-1} peak shifted to a higher wavelength after Cr doping [23].

CONCLUSION

Pure and Cr-doped TiO_2 NPs were successfully prepared using sol–gel method. Different Cr concentrations were used, and the morphological and structural properties of the prepared NPs were investigated by using FESEM, XRD, and FTIR. Cr-doped TiO_2 samples had smaller shapes compared to pure TiO_2. A mixed anatase and rutile phase was obtained Cr was added. The rutile phase started appearing at 1 wt% Cr and remained unchanged with increasing Cr concentration. Besides that, the crystallite size of anatase decreased from 69.55 to 17.39 nm for Cr-doped TiO_2 NPs due to the presence of rutile phase. The SSA increased and the crystallite size decreased when the Cr concentration increased. FTIR spectroscopy showed that the Ti–O–Ti vibration bands shifted to a higher wavelength with the addition of Cr. Based on these results, the suggested optimum value for Cr concentration is 1 wt%, which caused substantial changes on the structural properties of TiO_2 NPs.

ACKNOWLEDGEMENTS

The authors would like to thank Universiti Teknologi MARA (UiTM) for the financial support through the grant (No. 600-RMC/LESTARI SDG-T 5/3 (017/2021). The authors also acknowledge the Faculty of Applied Sciences and Institute of Science, UiTM for the experimental and characterization facilities.

REFERENCES

1. Ahmed, L. M., Ivanova, I., Hussein, F. H. & Bahnemann, D. W. (2014) Role of platinum deposited on TiO2 in photocatalytic methanol

oxidation and dehydrogenation reactions. *Int. J. Photoenergy*.

2. Chen, D., *et al.* (2020) Photocatalytic degradation of organic pollutants using TiO2-based photocatalysts: A review. *J. Clean. Prod.*, **268**, 121725.

3. Lucas, S. S., Ferreira, V. M. & De Aguiar, J. L. B. (2013) Incorporation of titanium dioxide nanoparticles in mortars - Influence of microstructure in the hardened state properties and photocatalytic activity. *Cem. Concr. Res.*, **43**, 112–120.

4. Fujishima, A., Zhang, X. & Tryk, D. A. (2007) Heterogeneous photocatalysis: From water photolysis to applications in environmental cleanup. *Int. J. Hydrogen Energy*, **32**, 2664–2672.

5. Rehman, F. U., Zhao, C., Jiang, H. & Wang, X. (2016) Biomedical applications of nano-titania in theranostics and photodynamic therapy. *Biomater. Sci.*, **4**, 40–54.

6. Leyva-Porras, C., *et al.* (2015) Low-temperature synthesis and characterization of anatase TiO2 nanoparticles by an acid assisted sol-gel method. *J. Alloys Compd.*, **647**, 627–636.

7. Hasan, F. (2019) Synthesis of Cr Doped TiO2 Using Sol-Gel Technique and Calculation of its Photocatalytic Activity.

8. Peng, Y. H., Huang, G. F. & Huang, W. Q. (2012) Visible-light absorption and photocatalytic activity of Cr-doped TiO 2 nanocrystal films. *Adv. Powder Technol.*, **23**, 8–12.

9. Zhou, X., Lu, J., Li, L. & Wang, Z. (2011) Preparation of crystalline Sn-Doped TiO2 and its application in visible-light photocatalysis. *J. Nanomater*.

10. Choudhury, B. & Choudhury, A. (2012) Dopant induced changes in structural and optical properties of Cr 3+ doped TiO2 nanoparticles. *Mater. Chem. Phys.*, **132**, 1112–1118.

11. Khaleel, A., Shehadi, I. & Al-Shamisi, M. (2010) Structural and textural characterization of sol-gel prepared nanoscale titanium-chromium mixed oxides. *J. Non. Cryst. Solids*, **356**, 1282–1287.

12. Mathews, N. R., Morales, E. R., Cortés-Jacome, M. A. & Toledo Antonio, J. A. (2009) TiO2 thin films - Influence of annealing temperature on structural, optical and photocatalytic properties. *Sol. Energy*, **83**, 1499–1508.

13. Muthee, D. K. & Dejene, B. F. (2021) Effect of annealing temperature on structural, optical, and photocatalytic properties of titanium dioxide nanoparticles. *Heliyon*, **7**, e07269.

14. Khalid Hossain, M., *et al.* (2017) Annealing temperature effect on structural, morphological and optical parameters of mesoporous TiO2 film photoanode for dye-sensitized solar cell application. *Mater. Sci. Pol.*, **35**, 868–877 .

15. Kumar, M. M., Badrinarayanan, S. & Sastry, M. (2000) Nanocrystalline TiO2 studied by optical, FTIR and X-ray photoelectron spectroscopy: Correlation to presence of surface states. *Thin Solid Films*, **358**, 122–130.

16. Nakhate, G. G., *et al.* (2010) Hydrothermally derived nanosized Ni-doped TiO2: A visible light driven photocatalyst for methylene blue degradation. *Mater. Chem. Phys.*, **124**, 976–981.

17. Prekajski, M., *et al.* (2016) Synthesis and characterization of Cr3+ doped TiO2 nanometric powders. *Ceram. Int.*, **42**, 1862–1869.

18. Dubey, R. S. & Singh, S. (2017) Investigation of structural and optical properties of pure and chromium doped TiO2 nanoparticles prepared by solvothermal method. *Results Phys.*, **7**, 1283–1288.

19. Irshad, K., Tahir Khan, M. & Murtaza, A. (2018) Synthesis and characterization of transition-metals-doped ZnO nanoparticles by sol-gel auto-combustion method.

20. Guo, W. L., Wang, X. K., Lin, Z. M. & Song, G. Z. (2002) Sonochemical Synthesis of Nanocrystalline TiO2 by Hydrolysis of Titanium Alkoxides. *Kao Teng Hsueh Hsiao Hua Heush Hsueh Pao/Chem. J. Chinese Univ.*, **23**, 1593–1594.

21. Kotsyubynsky, V., *et al.* (2017) Rod-like rutile nanoparticles: Synthesis, structure and morphology. *J. Nano Res.*, **50**, 32–40.

22. Demirci, S., *et al.* (2016) Synthesis and characterization of Ag doped TiO 2 heterojunction films and their photocatalytic performances. *Appl. Surf. Sci.*, **390**, 591–601.

23. Ghasemi, S., Rahimnejad, S., Setayesh, S. R., Rohani, S. & Gholami, M. R. (2009) Transition metal ions effect on the properties and photocatalytic activity of nanocrystalline TiO2 prepared in an ionic liquid. *J. Hazard. Mater.*, **172**, 1573–1578.